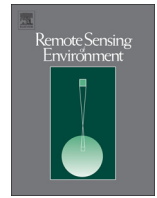


Contents lists available at [SciVerse ScienceDirect](#)

Remote Sensing of Environment

journal homepage: www.elsevier.com/locate/rse

Satellite derived euphotic depth in the Southern Ocean: Implications for primary production modelling

M.A. Soppa^{a,*}, T. Dinter^{a,b}, B.B. Taylor^a, A. Bracher^{a,b}^a Alfred-Wegener-Institut Helmholtz-Zentrum für Polar- und Meeresforschung, Bussestrasse 24, D-27570, Bremerhaven, Germany^b Institute of Environmental Physics, University of Bremen, PO Box 330440, D-28334 Bremen, Germany

ARTICLE INFO

Article history:

Received 17 December 2012

Received in revised form 21 June 2013

Accepted 23 June 2013

Available online xxxx

Keywords:

Euphotic zone

SeaWiFS

MODIS

Southern Ocean

Phytoplankton absorption

Ocean colour

ABSTRACT

The euphotic depth (Z_{eu}) is a key parameter in modelling primary production (PP) using satellite ocean colour. However, evaluations of satellite Z_{eu} products are scarce. The objective of this paper is to investigate existing approaches and sensors to estimate Z_{eu} from satellite and to evaluate how different Z_{eu} products might affect the estimation of PP in the Southern Ocean (SO). Euphotic depth was derived from MODIS and SeaWiFS products of (i) surface chlorophyll-a (Z_{eu} -Chla) and (ii) inherent optical properties (Z_{eu} -IOP). They were compared with *in situ* measurements of Z_{eu} from different regions of the SO. Both approaches and sensors are robust to retrieve Z_{eu} , although the best results were obtained using the IOP approach and SeaWiFS data, with an average percentage of error (E) of 25.43% and mean absolute error (MAE) of 0.10 m (log scale). Nevertheless, differences in the spatial distribution of Z_{eu} -Chla and Z_{eu} -IOP for both sensors were found as large as 30% over specific regions. These differences were also observed in PP. On average, PP based on Z_{eu} -Chla was 8% higher than PP based on Z_{eu} -IOP, but it was up to 30% higher south of 60°S. Satellite phytoplankton absorption coefficients (a_{ph}) derived by the Quasi-Analytical Algorithm at different wavelengths were also validated and the results showed that MODIS a_{ph} are generally more robust than SeaWiFS. Thus, MODIS a_{ph} should be preferred in PP models based on a_{ph} in the SO. Further, we reinforce the importance of investigating the spatial differences between satellite products, which might not be detected by the validation with *in situ* measurements due to the insufficient amount and uneven distribution of the data.

© 2013 Elsevier Inc. All rights reserved.

1. Introduction

Phytoplankton primary production (PP) is one of the key drivers regulating the ocean carbon cycle. In the Southern Ocean (SO), phytoplankton blooms develop with the retreat of sea ice in the springtime and, as a result, surface waters turn into a strong sink of CO₂ (Takahashi et al., 2009). Because PP has a high spatial and temporal variability within this part of the global ocean, it is difficult to assess and monitor it with *in situ* measurements. Despite the efforts to accurately estimate PP from ocean colour, studies showed large differences in the SO estimates (Campbell et al., 2002; Carr et al., 2006).

A common parameter shared by different ocean colour PP models is the euphotic depth (Z_{eu}). In biological terms, Z_{eu} is the bottom of the euphotic zone; the part of the water column with sufficient light for supporting photosynthesis and thus PP (Falkowski & Raven, 2007, chap. 9; Kirk, 2011, chap. 1). In physical terms, Z_{eu} is the depth where the downward photosynthetic available radiation (PAR), the radiation

in the spectral range of 400–700 nm, is reduced to 1% of its value beneath the surface (Morel & Berthon, 1989).

In ocean colour remote sensing Z_{eu} can be estimated (i) empirically from the surface chlorophyll-a concentration (Chla, Z_{eu} -Chla) (Morel, in Lee et al., 2007) and (ii) semi-analytically from the inherent optical properties of the water (IOPs, Z_{eu} -IOP) (Lee, Du, Arnone, Liew, & Penta, 2005). The main difference between the two approaches is that the derivation of Z_{eu} from Chla assumes that the optical properties of the optically active constituents co-vary with Chla (so-called Case 1 waters). On the other hand, the IOP approach determines the vertical distribution of light from the IOPs and therefore Z_{eu} can be retrieved in optically complex waters too, as shown by Lee et al. (2007) and Shang, Lee, and Wei (2011).

Uncertainties in Z_{eu} estimated from satellite data in the China Sea were investigated by Shang, Lee, et al. (2011). However, to our knowledge, there is no detailed evaluation of the satellite Z_{eu} in the SO. A comparison of ocean colour sensor/retrievals with *in situ* measurements, as well as the further impact on the PP modelling is thus necessary.

In this context, the main goal of this paper is to investigate the differences in estimating Z_{eu} from satellite remote sensing using different approaches and sensors in the SO. We compute Z_{eu} from ocean colour products of (i) Chla and (ii) IOP and validate those using *in situ*

* Corresponding author. Tel.: +49 471 4831 1785.

E-mail addresses: msoppa@awi.de (M.A. Soppa), dinter@iup.physik.uni-bremen.de (T. Dinter), bettina.taylor@awi.de (B.B. Taylor), astrid.bracher@awi.de (A. Bracher).

measurements of Z_{eu} . In addition, we compare Z_{eu} derived from the Moderate Resolution Imaging Spectroradiometer (MODIS) and the Sea-viewing Wide Field-of-view Sensor (SeaWiFS) sensors. The approaches and sensors are further examined in terms of the spatial distribution of Z_{eu} . Since phytoplankton absorption coefficient (a_{ph}) data are used in the PP calculation, we also examine the uncertainties of MODIS and SeaWiFS a_{ph} derived with the Quasi-Analytical Algorithm (QAA, Lee et al., 2005). Finally, we apply the absorption based primary production model (ABPM, Hirawake et al., 2011; Hirawake, Shinmyo, Fujiwara, & Saitoh, 2012) to investigate how different Z_{eu} products might affect the estimation of PP in the SO.

2. Material and methods

2.1. In situ data

A data set of *in situ* measurements of Chla (N = 1032) and Z_{eu} (N = 1288) in the SO was built to validate the satellite measurements. The data set compiled measurements from 1997 to 2008 taken by several investigators (Fig. 1 and Table A1). The Chla data were restricted to Chla derived from High Performance Liquid Chromatography (HPLC) pigment analysis, within 12 m surface layer and taken within 3 h of the Z_{eu} *in situ* measurements. An average value of Chla was calculated if two or more

samples were collected within the surface layer. We used Z_{eu} data provided in the databases that were calculated from *in situ* measurements of vertical profiles of PAR (N = 977). In addition, vertical profiles of PAR were also available in the SeaBASS database (cruises are marked with * in Table A1, Appendix) and those were used to calculate Z_{eu} (N = 311). We corrected surface measurements for wave perturbations when necessary as described in Taylor et al. (2011) and profiles not deep enough to reach the 0.01 of PAR at surface were discarded. A third data set of *in situ* measurements of a_{ph} (N = 465) was compiled to validate the a_{ph} derived from satellite remote sensing reflectance (R_{rs}). The a_{ph} data are derived from filter pad measurements taken in the years 2007, 2008, 2010 and 2012. The ANT-XXVI/3 and ANT-XXVIII/3 data were measured according to the filter pad method described in Taylor et al. (2011). Fig. 1 presents the relative frequency distribution of the Z_{eu} , Chla and spectrally averaged a_{ph} coefficient over 400–700 nm (\bar{a}_{ph} , see Section 2.4) *in situ* measurements that matched with SeaWiFS and MODIS data. Their relative frequency distribution by latitude and longitude is presented in the Appendix (Fig. A1).

2.2. Satellite data

MODIS-Aqua (R2012.0) and SeaWiFS (R2010.0) level 3 products of Chla (CHL1), PAR, R_{rs} were obtained at <http://oceancolor.gsfc.nasa.gov/>.

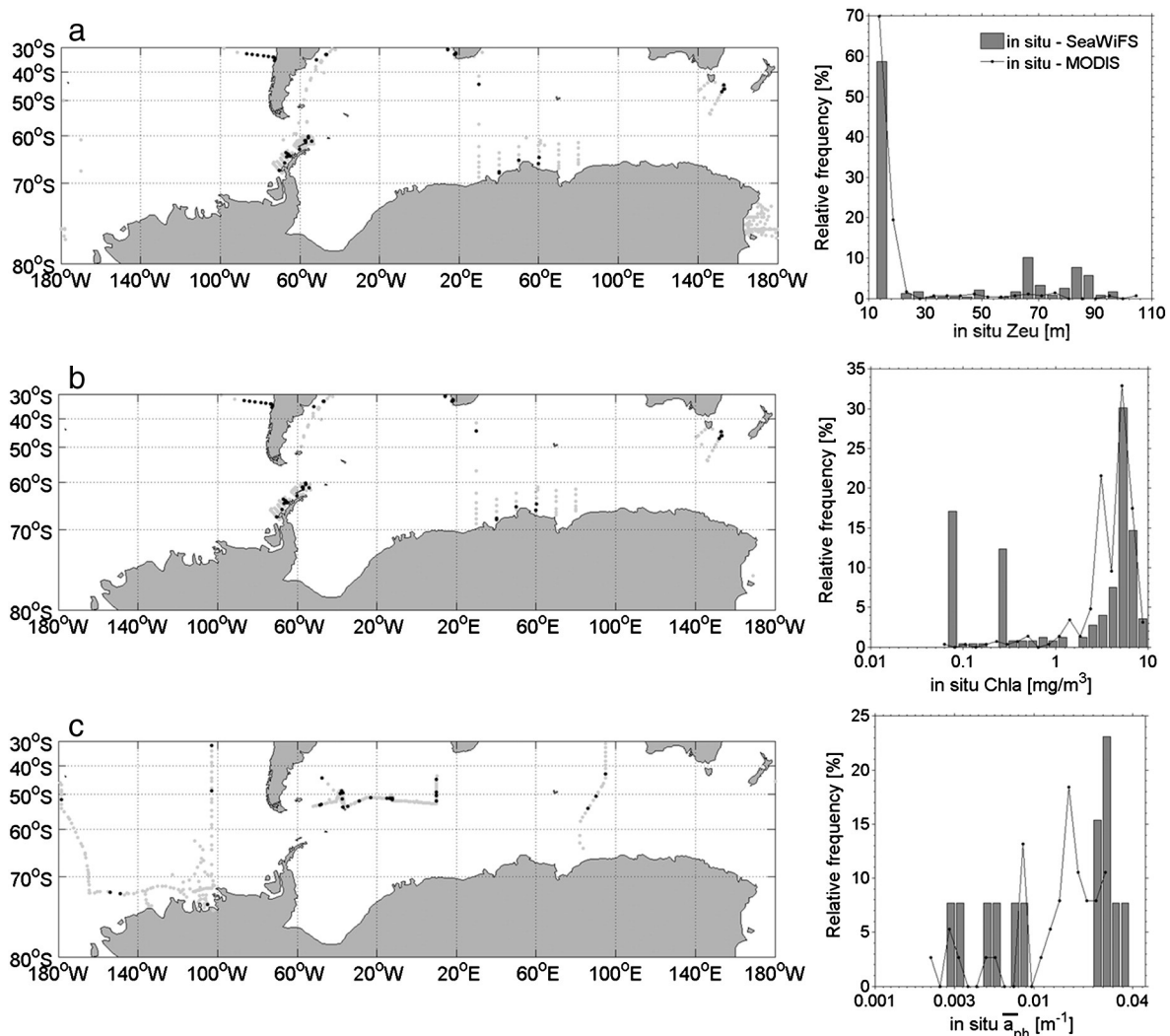


Fig. 1. On the left, location of the *in situ* measurements in light grey and the matched ones with satellite in black: (a) Z_{eu} , (b) Chla and (c) a_{ph} (\bar{a}_{ph}). On the right, the respective relative frequency distribution of the matched *in situ* measurements.

The data are produced and distributed by the NASA Goddard Space Flight Center's Ocean Data Processing System (ODPS). The SeaWiFS data set has the longest time series; however, the data acquisition ended in December 2010. We used MODIS and SeaWiFS data at $9 \times 9 \text{ km}^2$ spatial resolution. Satellite PAR and a_{ph} derived from R_{rs} (see Section 2.4) were used in the PP model. For the validation with *in situ* measurements daily images were used; for spatial distribution analysis we used monthly data.

2.3. Z_{eu} derived from ocean colour

Two approaches were used to derive Z_{eu} from ocean colour products. The approaches are briefly described below:

(i) Z_{eu} derived from Chla (Z_{eu} -Chla).

Based on the Case 1 waters assumption, the relationship is expressed as:

$$Z_{eu} = 34 \cdot (\text{Chla})^{-0.39} \quad (\text{Morel, in Lee et al., 2007}) \quad (1)$$

Standard CHL1 data are derived using the maximum band ratio (X) chlorophyll algorithms OC4v.6 (SeaWiFS) and OC3M (MODIS), defined as:

$$\log(\text{Chla}) = a_0 + a_1X + a_2X^2 + a_3X^3 + a_4X^4 \quad (2)$$

where for SeaWiFS,

$$X = \log \left[\frac{\max(R_{rs}(443), R_{rs}(490), R_{rs}(510))}{R_{rs}(555)} \right] \quad (3)$$

For MODIS two band ratios are used to replace the three band ratios in the SeaWiFS algorithm: $R_{rs}(443)/R_{rs}(550)$ and $R_{rs}(490)/R_{rs}(550)$. The coefficients a_0, a_1, a_2, a_3 and a_4 are 0.3272, -2.9940, 2.7218, -1.2259 and -0.5683 for SeaWiFS (Feldman & McClain, 2011) and 0.283, -2.753, +1.457, +0.659 and -1.403 for MODIS (O'Reilly et al., 2000).

(ii) Z_{eu} derived from the IOPs (Z_{eu} -IOP).

The QAA (version 5, Lee, Lubac, Werdell, & Arnone, 2009) was applied to derive the absorption and backscattering coefficients at 490 nm (a_{490} and b_{490}) from the satellite R_{rs} . Briefly, the QAA is an inversion algorithm that analytically derives the absorption and backscattering coefficients from the R_{rs} . First, the total absorption coefficient was calculated at a reference wavelength (λ_0 , 555 nm for SeaWiFS and 550 nm for MODIS) (Lee et al., 2009):

$$a(\lambda_0) = a_w(\lambda_0) + 10^{-1.146 - 1.366X - 0.469X^2} \quad (4)$$

where,

$$X = \log \left[\frac{r_{rs}(443) + r_{rs}(490)}{r_{rs}(\lambda_0) + 5 \frac{r_{rs}(667)}{r_{rs}(490)} \cdot r_{rs}(667)} \right] \quad (5)$$

Subsequently, the calculation was propagated to the other wavelengths. The vertical attenuation coefficient of PAR (K_{PAR}) was then derived from a_{490} and b_{490} . Z_{eu} was determined as:

$$Z_{eu} = \frac{4.605}{K_{PAR}(Z_{eu})} \quad (\text{Lee et al., 2007}) \quad (6)$$

Details on the algorithm and its uncertainties are presented in Lee et al. (2005), Lee, Carder, and Arnone (2006) and Lee, Arnone, Hu, Werdell, and Lubac (2010).

2.4. Primary production model

The net PP was calculated using the ABPM (Hirawake et al., 2011, 2012), an improved version of the Vertically Generalized Production Model (Behrenfeld & Falkowski, 1997) for polar oceans. In the ABPM, the product of the chlorophyll-*a* normalized maximum photosynthetic rate in the water column (P_{opt}^B , $\text{mg C (mg Chla)}^{-1} \text{ h}^{-1}$) and Chla (mg m^{-3}) is replaced by a linear relation of the spectrally averaged a_{ph} coefficient over 400–700 nm (\bar{a}_{ph} , m^{-1}). This model eliminates uncertainties of the satellite Chla product and the temperature effect on the estimation of the P_{opt}^B (Hirawake et al., 2011). The ABPM is expressed as:

$$NPP = 109.66 \cdot \bar{a}_{ph}(0^-) - 0.02 \cdot \frac{0.66125 \cdot E_0}{E_0 + 4.1} \cdot Z_{eu} \cdot D_{irr} \quad (7)$$

where E_0 is the daily integrated photosynthetic available radiation (PAR, $\text{Einsteins m}^{-2} \text{ day}^{-1}$) from satellite (see Section 2.2) and D_{irr} is the photoperiod (h) calculated as described in <http://orca.science.oregonstate.edu/faq01.php>. The PP estimated from Z_{eu} -Chla is represented as PP- Z_{eu} -Chla and from Z_{eu} -IOP as PP- Z_{eu} -IOP.

The QAA was applied to derive the a_{ph} at the SeaWiFS spectral bands of 412, 443, 490, 510 and 555 nm and MODIS spectral bands of 412, 443, 488, 531 and 555 nm. Satellite \bar{a}_{ph} were then derived by adjusting the a_{ph} integrated over the visible bands of SeaWiFS and MODIS to the *in situ* \bar{a}_{ph} over the continuous visible range (400–700) (Hirawake et al., 2011, 2012):

$$\bar{a}_{ph}(0^-) = \frac{a \cdot \sum_{N=1}^4 \left[\left(a_{ph}(\lambda_{i+1}) + a_{ph}(\lambda_i) \right) \cdot \left(\frac{\lambda_{i+1} - \lambda_i}{2} \right) \right]}{700 - 400} \quad (8)$$

where λ were the above mentioned spectral bands of SeaWiFS and MODIS. The parameter a represents the slope of the regression of the satellite \bar{a}_{ph} to the *in situ* \bar{a}_{ph} and corresponded to 1.3656 for SeaWiFS and 1.5354 for MODIS.

2.5. Validation and statistical analysis

The MODIS and SeaWiFS match ups were obtained when the day, latitude and longitude of the *in situ* observation fell within the limits of 1×1 pixel window. The bias, average absolute percentage of error (E), root mean square error (RMSE) and mean absolute error (MAE) were calculated to evaluate the differences between the *in situ* Z_{eu} and the satellite Z_{eu} :

$$\log_bias = \frac{1}{N} \sum_{i=1}^N (\log(Y_i) - \log(X_i)) \quad (9)$$

$$E = \left(\frac{1}{N} \sum_{i=1}^N \left| \frac{Y_i - X_i}{X_i} \right| \right) \cdot 100\% \quad (10)$$

$$\log_RMSE = \sqrt{\frac{1}{N} \sum_{i=1}^N (\log(Y_i) - \log(X_i))^2} \quad (11)$$

$$\log_MAE = \frac{1}{N} \sum_{i=1}^N |\log(Y_i) - \log(X_i)| \quad (12)$$

where X was the *in situ* value, Y the satellite value and N is the number of matching pairs. The statistical indicators \log_bias , E and \log_RMSE were chosen based on the GlobColour Validation Report (2007) and other literatures on satellite validation (e.g. Zibordi, Melin, & Berthon, 2006; Shang, Lee, et al., 2011). The \log_MAE was used as a statistical estimator of error for comparisons between the sensors and a_{ph} at different wavelengths, since N changes. Willmott and Matsuura (2005) showed that RMSE is sensitive to the square root of N and MAE should be preferred instead. No outliers were removed. For reference, a 1:1 line was included in the scatterplots to show how well the satellite and *in situ* data agree.

Monthly climatologies of Z_{eu} and PP in December, January and February, were computed to investigate spatial differences. The climatology fields were calculated from monthly images for the 2003–2009 period, excluding the year of 2008 when SeaWiFS did not acquire data. For each pixel, the relative difference between the spatial fields was derived:

$$DIFF = \left(\frac{A-B}{B} \right) \cdot 100\% \quad (13)$$

where A corresponded to Z_{eu} -Chla, Z_{eu} -SWF or PP- Z_{eu} -Chla and B to Z_{eu} -IOP, Z_{eu} -MODIS or PP- Z_{eu} -IOP. We did not compare the spatial distribution of PP between the sensors because $\bar{\alpha}_{ph}$, PAR and Chla might introduce differences in the PP estimation.

3. Results

3.1. Comparison of satellite and in situ Z_{eu}

Fig. 2 presents the comparison between satellite and *in situ* Z_{eu} . The overall statistics show that the two approaches agree well with the *in situ* measurements. When Z_{eu} -SWF was derived by the IOP approach, the statistics are slightly better than Z_{eu} -Chla improving the *E* in 3.5% (Fig. 2a and b) and the regression line is close to the 1:1 line (dotted line). On the other hand, Z_{eu} -Chla shows better results than Z_{eu} -IOP for MODIS, reducing the *E* in 9.5% (Fig. 3c and d). Differences in log₁₀MAE indicate that Z_{eu} retrieved from SeaWiFS is more

accurate than MODIS. Negative biases are found for Z_{eu} -MODIS and positive biases for Z_{eu} -SWF.

Compared to collocated *in situ* HPLC Chla data of our validation data set, the standard SeaWiFS algorithm (OC4v.6) underestimates Chla (Fig. 3). For MODIS, the OC3M algorithm leads to under- and overestimation of Chla depending on the *in situ* Chla. For *in situ* Chla < 1.5 mg/m³, Chla was on average underestimated, whereas for higher concentrations (> 1.5 mg/m³) the retrievals were overestimating the *in situ* values.

3.2. Spatial distribution of Z_{eu} -Chla and Z_{eu} -IOP

Fig. 4 presents the spatial distribution of the climatology of Z_{eu} for February, using data from 2003 to 2009. Deeper Z_{eu} are associated with oligotrophic waters in the zonal band of 30°–40°S. Shallower Z_{eu} are observed in the waters around the Antarctic continent, South America, south and west part of South Africa and between 40°–50°S, except for the eastern Pacific Sector. Shallower Z_{eu} is related to terrigenous influence (e.g. La Plata river plume in the Patagonian Shelf region) and higher chlorophyll concentrations in upwelling regions (e.g. Benguella upwelling), polar fronts, islands (e.g. Kerguelen islands) and continental shelves (e.g. Antarctic Peninsula). The dynamic of Chla in the SO was recently investigated by Thomalla, Fauchereau, Swart, and Monteiro (2011). For comparison, the spatial distribution of Z_{eu} in February 2003 is presented in the Appendix and shows that there are no major differences between monthly and climatology maps (Fig. A2). The difference

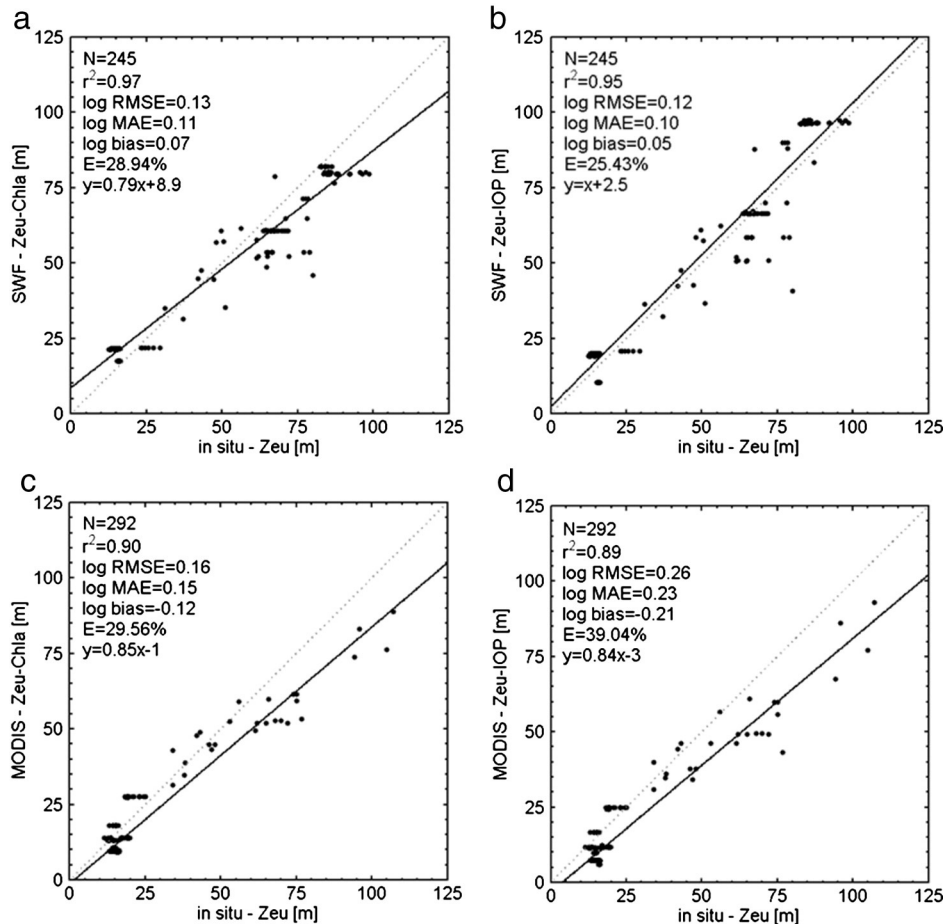


Fig. 2. Scatterplots of satellite Z_{eu} against *in situ* Z_{eu} . (a) and (c) Z_{eu} is derived from Chla approach (Z_{eu} -Chla), (b) and (d) Z_{eu} is derived from the IOP approach (Z_{eu} -IOP). The solid line represents the regression and the dotted line represents 1:1 line as reference.

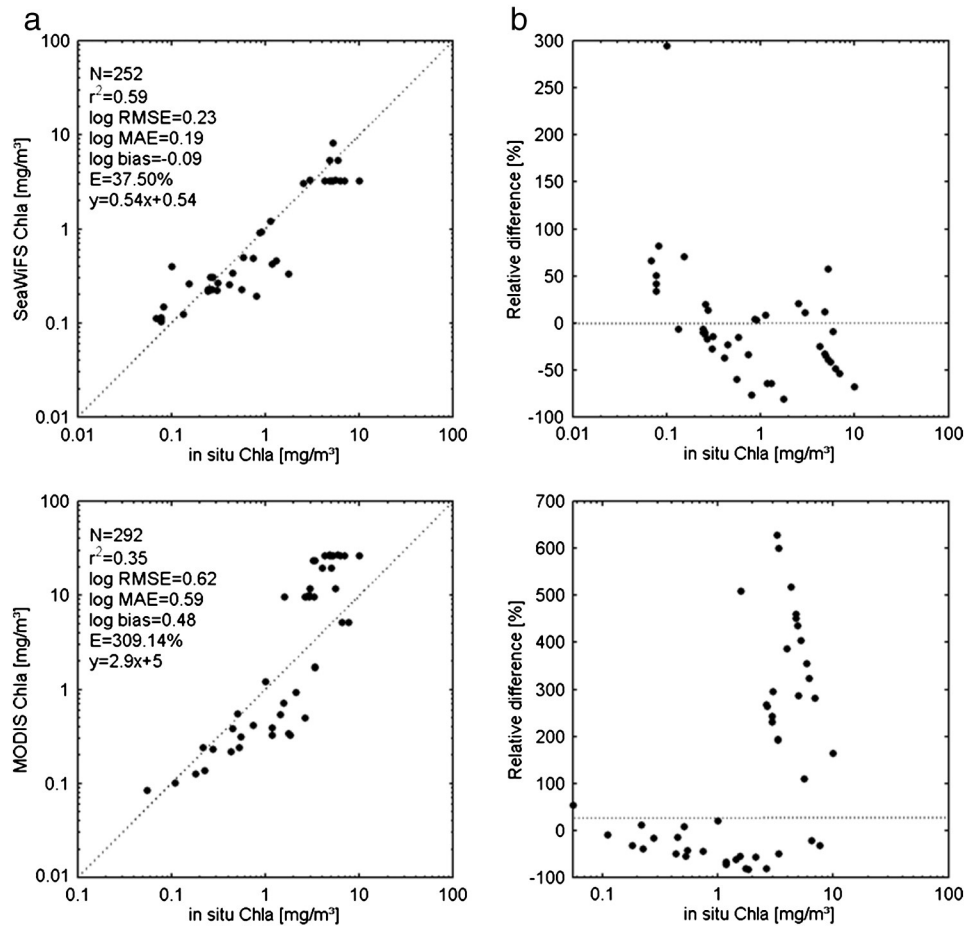


Fig. 3. (a) Scatterplots of satellite and *in situ* Chla. The dotted line represents the 1:1 line as reference. (b) Relative differences between satellite Chla and *in situ* Chla. The dotted line represents the zero line.

in calculating the climatology of Z_{eu} from daily or monthly images was small as well. For instance, the standard deviations of the difference between Z_{eu} -Chla calculated from daily data and monthly data in February 2003 are 1.22 m for SWF and 1.08 m for MODIS. For the IOP approach the values are 0.91 m for SeaWiFS and 0.77 m for MODIS.

When Z_{eu} -Chla was compared with Z_{eu} -IOP, large differences were observed. While the range of Z_{eu} -Chla from SeaWiFS varies between 5.97 and 234.31 m (median = 65.50 m), using the IOP approach this range is much narrower, from 2.5 to 150 m (median = 63.93 m). Similar for MODIS, Z_{eu} -Chla varies between 5.89 and 259.69 m (median = 65.50 m) and Z_{eu} -IOP from 3.5 to 146.3 m (median = 62.37 m). On average, for the entire region, Z_{eu} -Chla from SeaWiFS and MODIS are 3.61 and 5.41% deeper than Z_{eu} -IOP. These differences followed a zonal distribution. The most notable difference was observed in the Pacific Sector within the 30°–40°S zonal band, corresponding to the South Pacific subtropical gyre, where Z_{eu} -Chla is ~20–30% deeper than Z_{eu} -IOP. The spatial distribution maps also pointed out differences of about 10–15% south of 60°S, with Z_{eu} -Chla usually deeper than Z_{eu} -IOP; especially for MODIS. Regions corresponding to deeper Z_{eu} -IOP were also presented, but they were less abundant and only about ~10% deeper.

Comparing the sensors, the spatial distribution of Z_{eu} is similar in both approaches, with an average difference (DIFF) of -0.005 and 2.68% for Z_{eu} -Chla and Z_{eu} -IOP, respectively in February (Fig. 5). However, the spatial differences are larger south of 60°S and more evident in Z_{eu} -IOP. A corresponding pattern was observed in December and

January. As to the spatial distribution of Z_{eu} , no major differences between monthly and climatology maps of DIFF were found (Fig. A3).

3.3. Net primary production

3.3.1. Validation of SeaWiFS and MODIS derived phytoplankton absorption coefficients

The ocean colour PP model used here is a function of \bar{a}_{ph} . The \bar{a}_{ph} can be determined empirically through linear relations between *in situ* \bar{a}_{ph} and satellite a_{ph} integrated over the visible spectral bands of SeaWiFS and MODIS. Hirawake et al. (2011, 2012) calculated these relationships based on a_{ph} derived from ship R_{rs} at the MODIS and SeaWiFS spectral bands, using the QAA. However, within this study the satellite R_{rs} derived a_{ph} were not validated due to the insufficient number of collocations between satellite and *in situ* data. Furthermore, to our knowledge, there is no information on the performance of the QAA to derive a_{ph} from satellite R_{rs} in the SO. Therefore, before we investigated the PP, we briefly assessed the quality of the a_{ph} derived from SeaWiFS and MODIS R_{rs} using the QAA with *in situ* a_{ph} . Results are presented in Table 1.

The log_MAE and E of a_{ph} -SWF increase for increasing wavelengths (except at 555 nm) and negative biases indicate an underestimation of a_{ph} . Results for MODIS show similar log_MAE and E at 412, 443 and 488 nm, increasing towards 555 nm. Negative a_{ph} values were retrieved at SeaWiFS bands 490, 510 and 555 and at MODIS bands 412 and 443 nm and lead to small but negative \bar{a}_{ph} . Those values were removed before the

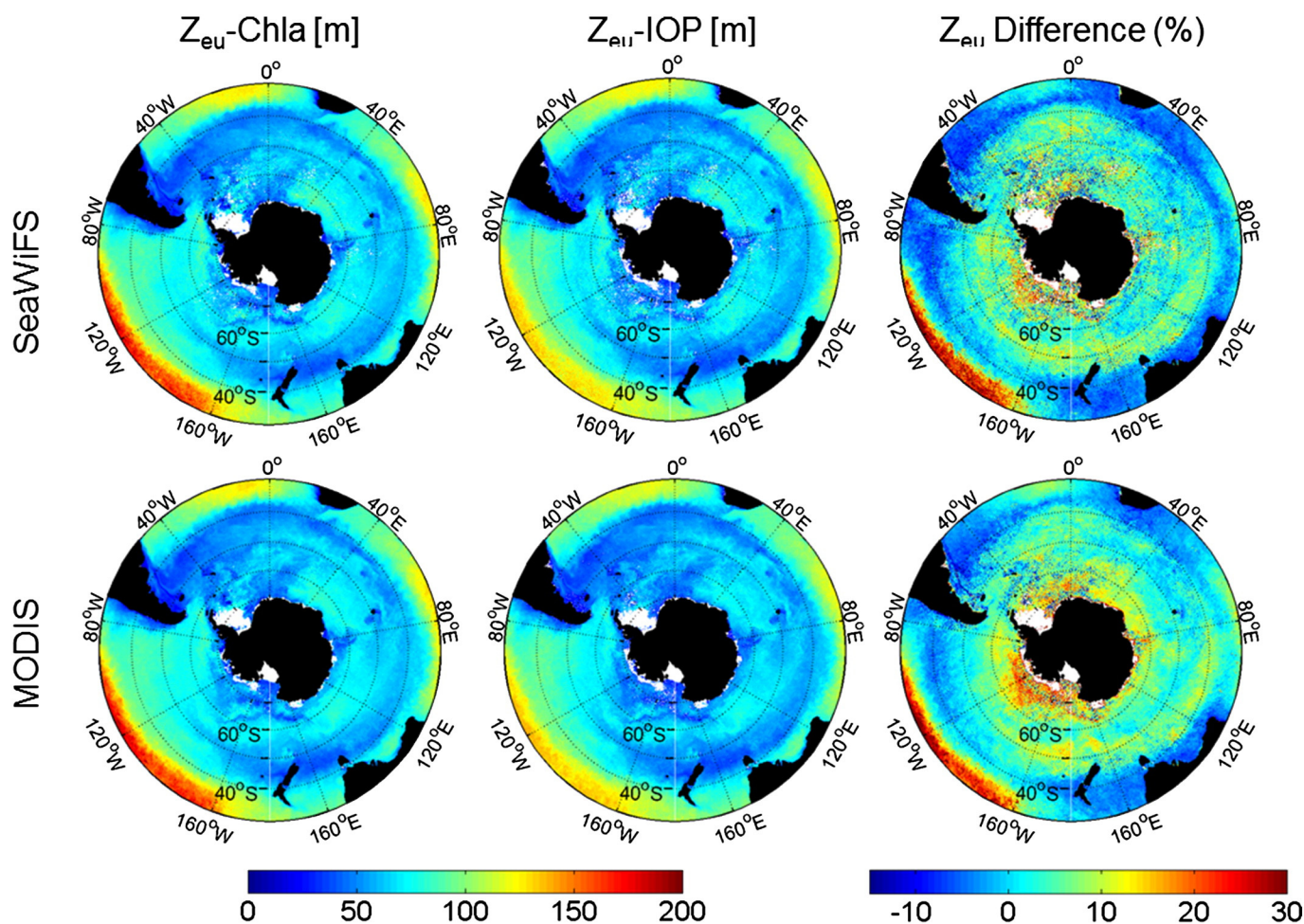


Fig. 4. Spatial distribution of Z_{eu} in the Southern Ocean (climatology of February). The white pixels correspond to areas with no data.

calculation of the statistics presented in Table 1. Estimates of PP on pixels with negative $\bar{\alpha}_{ph}$ were removed as well.

3.3.2. Spatial distribution of PP- Z_{eu} -Chla and PP- Z_{eu} -IOP

Generally, higher PP- Z_{eu} -Chla than PP- Z_{eu} -IOP was observed using both sensors over the SO (Fig. 6). For SeaWiFS PP- Z_{eu} -Chla was 7% higher than PP- Z_{eu} -IOP and for MODIS 10.22% higher. The average of PP- Z_{eu} -Chla and PP- Z_{eu} -IOP was 321.18 and 283.84 $\text{mg C m}^{-2} \text{d}^{-1}$ for SeaWiFS, respectively. Using MODIS data the PP- Z_{eu} -Chla and PP- Z_{eu} -IOP were 438.50 and 393.78 $\text{mg C m}^{-2} \text{d}^{-1}$, respectively. The corresponding monthly data for February 2003 are presented in the Appendix (Fig. A4). Although these differences may not be significant for studies focussing on the entire SO, for local comparisons they are relevant. For instance, in the region south of 60°S (60°S – 80°S , 120°W – 160°W) PP- Z_{eu} -Chla was $\sim 30\%$ higher than PP- Z_{eu} -IOP.

4. Discussion

4.1. Validation of Z_{eu} and Chla

This study investigated the differences between two approaches to derive satellite Z_{eu} : the first one by Morel (in Lee et al., 2007) is empirical and based on Chla and the second one by Lee et al. (2005) is semi-analytical and based on IOPs. We focussed on the Chla approach because of its simplicity, but also to investigate if the known inaccuracy of the standard satellite Chla products in the SO would impact the Z_{eu}

retrieval. The SO is heterogeneous in terms of bio-optical conditions. It comprises not only oligotrophic waters, but ultra-oligotrophic waters (e.g. South Pacific Gyre), complex waters (e.g. high CDOM and sediment in the Patagonia Shelf), upwelling regions (e.g. Benguela upwelling), polar fronts and coastal Antarctic waters (e.g. Antarctic Peninsula). For this reason, we included a more complex approach in our investigation: the IOP approach, which accounts for the vertical distribution of other in-water components that also contribute to the light attenuation. The QAA can be applied globally, regardless of the optical complexity of the water and has been widely used and cited in the literature.

Our validation data set covered a wide range of bio-optical conditions (Fig. 1); however uncertainties in Z_{eu} were only improved by the IOP approach for SeaWiFS (Fig. 2).

This observation agrees with Lee et al. (2007). The authors compared *in situ* Z_{eu} with Z_{eu} -Chla and Z_{eu} -IOP calculated from ship borne R_{rs} in the Monterey Bay, the Gulf of Mexico and the Arabian Sea and reported improved Z_{eu} from the IOP approach. In addition, Shang, Lee, et al. (2011) and Shang, Dong, Lee, Li and Behrenfeld (2011) studied oligotrophic and coastal waters of the South China Sea using MODIS data and showed that Z_{eu} -IOP was more accurate than empirically deriving Z_{eu} from Chla (Morel, Claustre, Antoine, & Gentili, 2007). Within MODIS data, our Z_{eu} estimation with the Chla approach yielded better results than the IOP approach.

Our results indicate that Z_{eu} can be accurately estimated by both approaches and sensors with a log₁₀ MAE within 0.10 and 0.23 m. The relative consistency observed between the sensors is related to the common processing schemes applied, such as the atmospheric correction and data

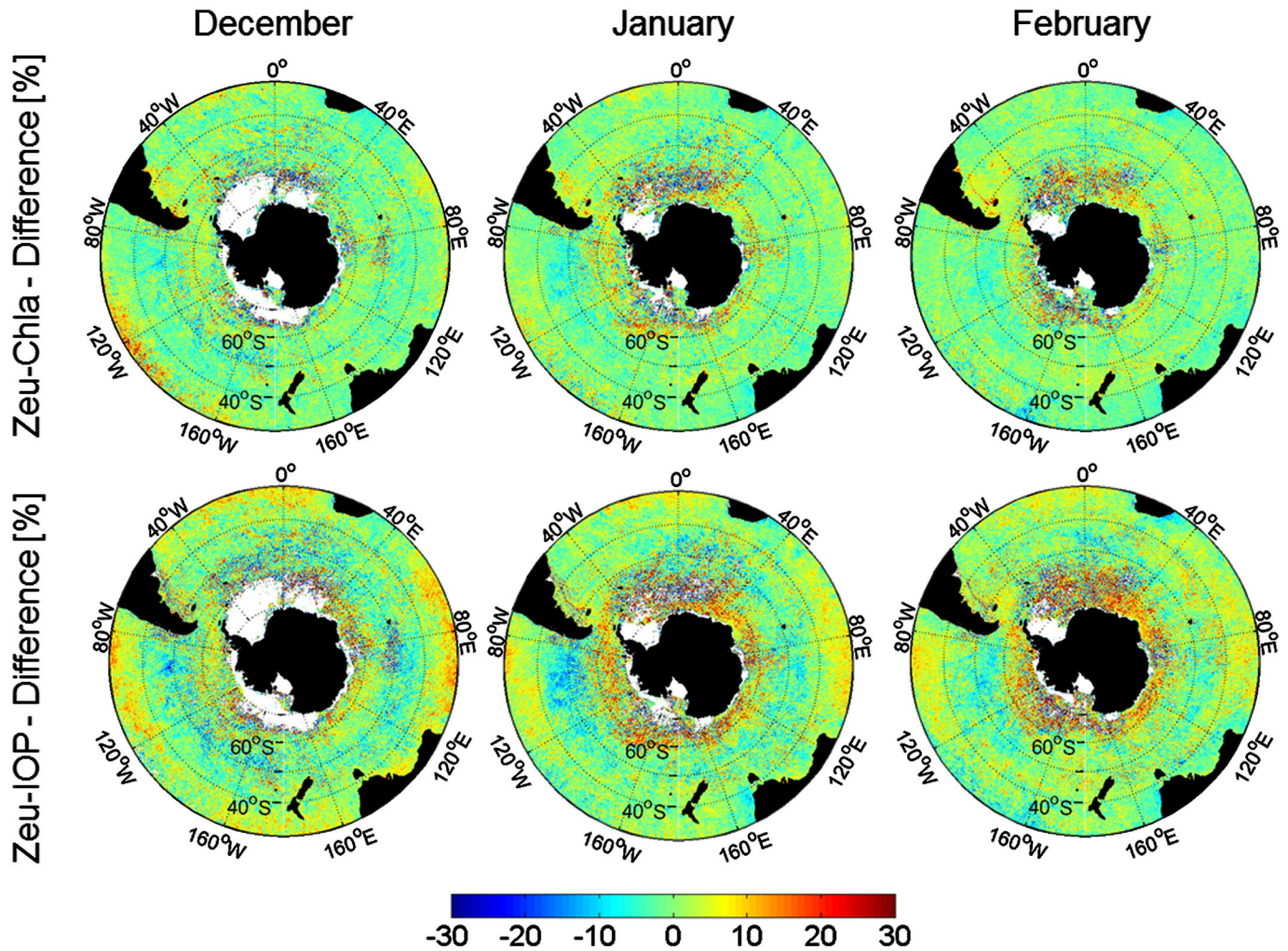


Fig. 5. Spatial distribution of the relative percentage of difference between SeaWiFS and MODIS. The white pixels correspond to areas with no data.

binning, as already pointed out by Mélin (2011). Differences might be caused by the granularity and coverage areas, spectral bands, orbital characteristics and equator crossing times. MODIS-Aqua crosses the equator at ~13:30 pm. For SeaWiFS the equator crossing time drifted throughout the mission, from 12:00 to 14:20, but 12:30 pm was used for the calculations. Additional sources of error in the validation analysis include the *in situ* measurements, as the use of different field sensors and data/sample processing.

Table 1
Statistical results of the comparison between QAA-satellite derived a_{ph} and *in situ* a_{ph} .

Wavelength (nm)	r^2	log_MAE	log_bias	E (%)	Satellite	Range	
						<i>In situ</i>	
<i>SeaWiFS</i> (N = 13)							
412 (N = 13)	0.79	0.21	-0.16	37.55	0.002–0.149	0.007–0.110	
443 (N = 13)	0.57	0.22	-0.11	44.90	0.003–0.171	0.007–0.092	
490 (N = 12)	0.23	0.27	-0.03	75.52	0.008–0.119	0.003–0.056	
510 (N = 12)	0.12	0.45	-0.28	89.31	0.001–0.083	0.001–0.054	
555 (N = 12)	0.40	0.35	-0.28	57.01	0.0003–0.042	0.001–0.002	
\bar{a}_{ph} (N = 12)	0.50	0.22	-0.10	47.40	0.005–0.076	0.003–0.034	
<i>MODIS</i> (N = 38)							
412 (N = 36)	0.34	0.18	-0.04	45.51	0.009–0.066	0.004–0.056	
443 (N = 36)	0.33	0.17	-0.005	48.93	0.011–0.079	0.005–0.064	
488 (N = 38)	0.38	0.18	-0.035	47.26	0.004–0.050	0.003–0.047	
531 (N = 38)	0.38	0.22	0.01	62.21	0.001–0.025	0.0001–0.025	
555 (N = 38)	0.21	0.50	0.50	406.41	0.009–0.025	0.0004–0.014	
\bar{a}_{ph} (N = 36)	0.44	0.16	0.06	53.08	0.006–0.038	0.002–0.030	

Results of the Chla validation indicate that the satellite CHL1 products from SeaWiFS are more accurate than from MODIS in the SO (Fig. 3). Our MODIS validation data set is, however, biased towards high Chla waters (Fig. 1); 95% of the *in situ* data had Chla > 1 mg/m³ where the errors are generally higher as well. In contrast, the SeaWiFS validation data set has only 65% of samples at Chla > 1 mg/m³. For instance, the difference in the log_MAE between MODIS and SeaWiFS for Chla < 1 mg/m³ is 0.02 mg/m³ (0.17 mg/m³ for MODIS and 0.15 mg/m³ for SeaWiFS); for higher concentrations this difference increases to 0.4 mg/m³ (0.61 mg/m³ for MODIS and 0.21 mg/m³ for SeaWiFS). The observed underestimation of Chla by the operational SeaWiFS and MODIS algorithms (here only for Chla < 1.5 mg/m³) is in accordance with previous studies that used earlier algorithm versions, indicating that this issue still persists in the SO (Dierssen & Smith, 2000; Garcia, Garcia, & McClain, 2005; Kahru & Mitchell, 2010; Szeto, Werdell, Moore, & Campbell, 2011). Further, it is important to mention that we used surface Chla (see Section 2.1) instead of the weighted Chla in first optical depth. Our coincident *in situ* measurements of HPLC Chla profiles, K_d and Z_{eu} were all concentrated in the Antarctic Peninsula region, which represents a particular region of the SO, thus we used surface Chla values only. Moreover, we avoided the use of fluorometric data in our study and used HPLC data. Marrari, Hu, and Daly (2006) showed that the chlorophyll fluorescence of accessory pigments (e.g. chlorophyll-b) interferes in the determination of Chla by fluorometric methods in the SO.

Nevertheless, uncertainties of the satellite Chla have some but small influence on the Z_{eu} -Chla, which is in part linked to the nature of the power function that empirically relates Z_{eu} to Chla. One has

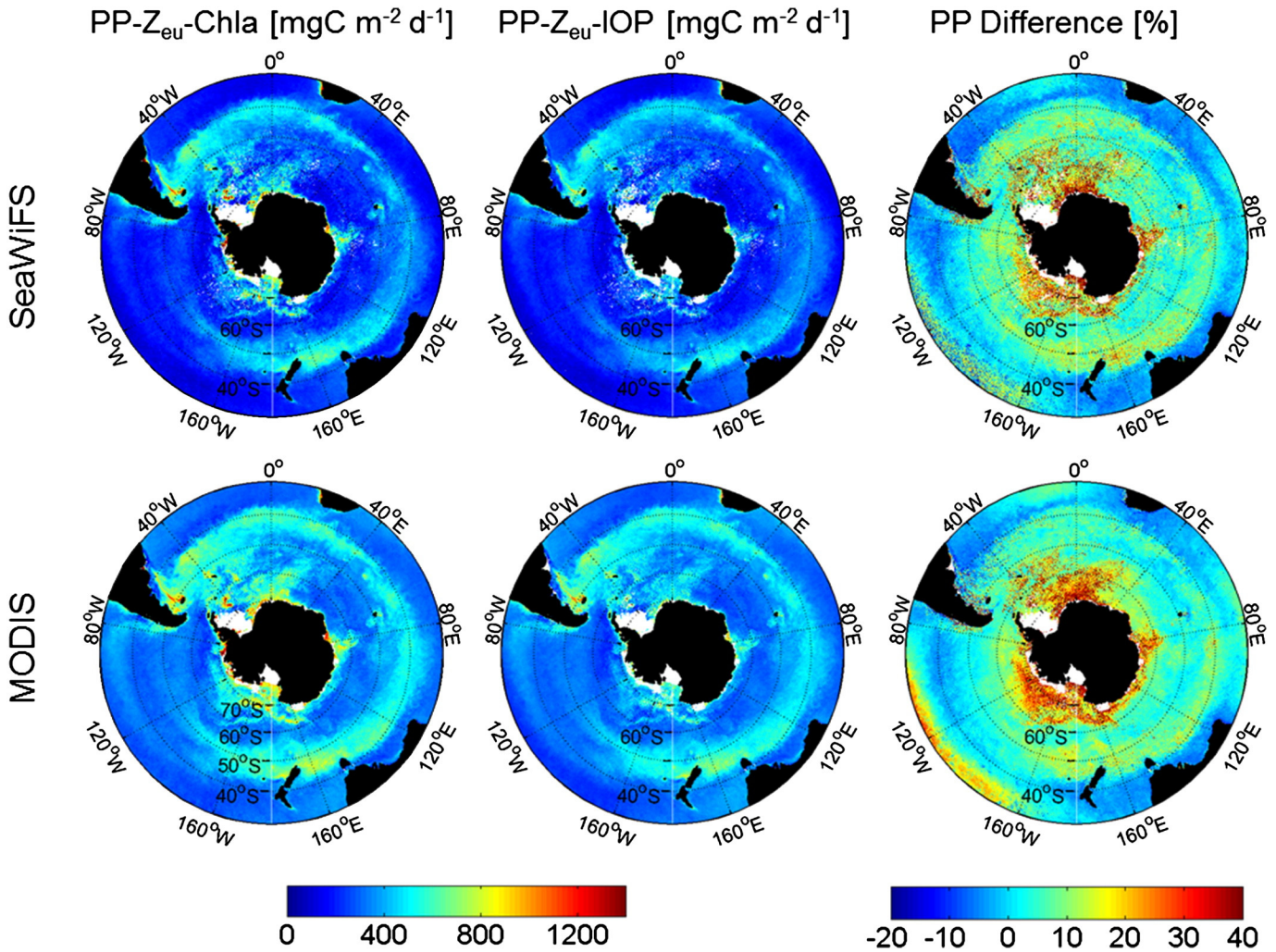


Fig. 6. Spatial distribution of PP in the Southern Ocean (climatology of February). PP-Z_{eu}-Chla (left), PP-Z_{eu}-IOP (right) and relative percentage of difference between PP-Z_{eu}-Chla and PP-Z_{eu}-IOP (center). The white pixels correspond to areas with no data.

to note that we used the CHL1 even in waters that hardly fit to the Case 1 assumption, for instance on the Patagonian shelf and around the Antarctic Peninsula (Dierssen & Smith, 2000; Garcia et al., 2005). The error in Z_{eu} induced by the error in Chla depends on the *in situ* concentrations. A 100% error in lower Chla values has higher impact on Z_{eu} than 100% error in high Chla values. For instance, a 100% overestimation in the lowest and highest *in situ* Chla (0.05 mg/m³ and 9.98 mg/m³) of our SeaWiFS validation data set would lead to an error of 26.79 and 2.82 m in Z_{eu}, respectively.

4.2. Zeu spatial distribution

The spatial distribution maps of Z_{eu}-Chla and Z_{eu}-IOP highlighted large differences in the South Pacific subtropical gyre and south of 60°S (Fig. 4). Morel et al. (2007) evaluated the Chla approach for waters of the South Pacific subtropical gyre with data collected during the BIOSOPE cruise and showed that an empirical relationship based on Chla (Morel & Gentilini, 2004) was valid to estimate Z_{eu} in those waters. Thus, for this region the satellite Z_{eu}-Chla may be the better choice. Unfortunately, beside the data from the BIOSOPE cruise, there were no *in situ* measurements of Z_{eu} available from the South Pacific and other SO subtropical gyres for a detailed investigation. Our comparison between satellite and *in situ* Z_{eu} for data south of 60°S did not show significant differences between the approaches for SeaWiFS and slightly better estimates of Z_{eu}-Chla for MODIS (see the Appendix for scatterplots, Fig. A5).

Overall, Z_{eu}-IOP was shallower than Z_{eu}-Chla, as observed by Lee et al. (2007) for other regions.

Although the spatial distribution of Z_{eu} is consistent, it is important to mention that close to the Antarctic continent the values might be impacted by ice contamination. Pixels contaminated by cloud/ice and straylight are flagged in the Level-3 data. Nevertheless, Belanger, Ehn, and Babin (2007) and Wang and Shi (2009) showed that the standard SeaWiFS and MODIS flags may not remove all pixels impacted by the adjacency effect, sub-pixel ice and mixed ice-water contamination. Based on radiative transfer simulations Belanger et al. (2007) showed the significant impact of the adjacency effect and sub-pixel ice contamination on the water leaving radiance and derived Chla and IOP products. In general, the sub-pixel contamination leads to an overestimation of Chla and the total absorption at 443 nm (*a*₄₄₃). The adjacency effect overestimates Chla in low Chla waters (0.05 mg m⁻³) and for Chla > 0.5 mg m⁻³, *a*₄₄₃ and Chla retrievals are underestimated. Wang and Shi (2009) observed that MODIS Chla is often overestimated in sea ice contaminated pixels. Therefore, both shallower and deeper Z_{eu} regions observed close to the Antarctic continent might be biased.

In addition, when comparing the sensors, the spatial differences were larger close to the sea ice edge and were likely related to the few pixels sampled at different times (Fig. 5). These differences were as large as 20% and more pronounced in the Z_{eu}-IOP, which might be explained by the following reasons. The IOP approach is probably more influenced by the atmospheric correction since the QAA uses the

670 nm band to derive the total absorption at the reference wavelength. The 670 nm band is important for the retrievals of IOPs from R_{rs} in high-absorption waters (Lee et al., 2006, 2007). At 670 nm water absorption dominates and the signal to noise ratio is low, which in turn leads to a high sensitivity to light conditions. This is also the most likely reason for the large differences seen south of 60°S (Figs. 4 and 5). Moreover, differences between Z_{eu} -SWF and Z_{eu} -MODIS might be associated to changes in the QAA depending on the sensor used. Examples of the QAA adjustment to sensors are the difference in reference wavelength (555 nm for SeaWiFS and 547 nm for MODIS) and the constants used to derive total absorption at the reference wavelength. These are based on relations to a different set of collocations and the solar zenith angle. An alternative is the use of merged products (e.g. GlobColour), aimed to reduce discrepancies caused by the use of different sensors as observed here.

4.3. Validation of a_{ph}

The assessment of MODIS and SeaWiFS QAA-derived a_{ph} is presented in Table 1. The comparison of R_{rs} -satellite and *in situ* a_{ph} shows satisfactory results in terms of log_MAE for both sensors at 412 and 443 nm, and at 488 and 531 for MODIS. The percentage differences are higher than the values presented by Lee et al. (2011). Nevertheless, Lee et al. (2011) derived a_{ph} from ship borne R_{rs} instead of satellite R_{rs} ; larger uncertainties would be expected in satellite R_{rs} . The E of a_{ph} -MODIS at 412, 443 and 488 were higher than the values reported by Shang, Dong, et al. (2011) when evaluating QAA-derived a_{ph} from satellite MODIS R_{rs} in the Taiwan Strait as well. Generally, a_{ph} -MODIS showed lower log_bias and log_MAE (except at 555 nm) than a_{ph} -SWF for the same wavelengths. Further, the comparison of log_MAE from the Chla and a_{ph} 443 validations suggested improvement of a_{ph} 443 over Chla in the SO for MODIS, as observed by Shang, Dong, et al. (2011) in the Taiwan Strait. Thus, MODIS should be preferred in PP models based on a_{ph} that use either a_{ph} 443 or \bar{a}_{ph} .

Uncertainties in the satellite a_{ph} could be introduced by error in the *in situ* measurements of a_{ph} , as well as in the satellite R_{rs} and in the estimation of *gelbstoff* absorption by the QAA (Lee et al., 2006, 2011, Shang, Dong, et al., 2011). Unfortunately, it is out of the scope of this paper to propose modifications in the algorithm for the SO. Hirawake et al. (2011) modified the QAA based on underwater spectral radiation data and *in situ* a_{ph} from the Indian Sector of the SO. This modified QAA was also tested by us, but the results were less robust than with the original QAA (results not shown). In part, regional differences across the SO, as discussed above and as seen in the Z_{eu} , make it difficult to extrapolate local properties to the entire region.

Because Z_{eu} -IOP was calculated using the same approach as a_{ph} 490(488), we could also expect an improvement of Z_{eu} -IOP over Z_{eu} -Chla; particularly for MODIS that showed a larger difference between the two Z_{eu} approaches. However, this was not observed here and it is likely related to our validation data sets of Z_{eu} and a_{ph} , which greatly differ in number of samples and location. Moreover, our a_{ph} validation data set is small, especially for SeaWiFS. From 271 *in situ* a_{ph} collected between 2007 and 2010, 13 matched with SeaWiFS observations. Persistent cloudiness and high solar zenith angles limit the satellite retrievals in the SO.

4.4. Primary production

Finally, the impact of the Z_{eu} products on the PP was as expected; deeper Z_{eu} led to an increase in PP as more light was available (Fig. 6). Note that the classification of empirical and semi-analytical used for Z_{eu} is not valid for PP since both PP- Z_{eu} -Chla and PP- Z_{eu} -IOP used a_{ph} derived from QAA. The spatial differences observed between Z_{eu} -Chla and Z_{eu} -IOP strongly influenced the PP estimation. In both PP calculations we used the same set of input data (PAR, D_{irr} , \bar{a}_{ph}), except for Z_{eu} , thus the

observed differences can be directly attributed to Z_{eu} . In particular, PP- Z_{eu} -Chla estimates were much higher than PP- Z_{eu} -IOP in the west part of the South Pacific subtropical gyre and south of 60°S. The latter region is of great importance in the global carbon cycle, as pointed out by Arrigo, van Dijken, and Long (2008) and Takahashi et al. (2009). According to these authors, once the sea ice retreats in springtime, more light and nutrients become available enhancing the development of phytoplankton blooms and leading to a strong sink of atmospheric CO₂. Accurate estimates of PP are essential for a better understanding of the role of the SO in the global carbon cycle.

From the results presented here it becomes clear that the uncertainties of Z_{eu} should be considered to improve the estimates of PP. Saba et al. (2011) investigated how satellite derived sea surface temperature, mixed layer depth, Chla and PAR affected the PP estimates of 21 ocean colour models. They found that when uncertainties of the Chla are accounted for in PP models, the root mean square difference is reduced by 44% in the Antarctic Polar Front Zone. They also observed that biases in the ocean colour PP estimates are related to the water column depth, possibly due to uncertainties in the Z_{eu} .

5. Summary and conclusions

This paper provides the first quality assessment of the Z_{eu} and a_{ph} products of MODIS and SeaWiFS using a large data set of *in situ* measurements in the SO. In summary, satellite Z_{eu} derived using the Chla and IOP approaches are reliable in the SO. Although uncertainties depend on the sensor and approach used, the best results were obtained by the IOP approach and SeaWiFS data. Within the MODIS data, Z_{eu} estimation with the Chla approach generally yielded better results than the IOP approach. When assessing the differences in the spatial distribution between Z_{eu} -Chla and Z_{eu} -IOP, large discrepancies were observed over specific regions with significant impact on the PP retrievals. Those differences were not observed in the validation. Therefore, we emphasize the importance of spatial studies together with the validation using *in situ* measurements for comparing ocean colour satellite products retrieved from different sensors and approaches. In addition, temporal differences should also be accounted for. Further, we validated a_{ph} and found that MODIS data lead to lower uncertainties of \bar{a}_{ph} and a_{ph} 443 than SeaWiFS data. Thus, MODIS should be preferred in PP models based on a_{ph} in the SO.

Our validation showed that the best satellite retrievals of Z_{eu} and \bar{a}_{ph} in the SO are not from the same sensor. To which extend these results are influenced by the lack of *in situ* measurements in our data set and/or by regional differences in the SO is still unclear. To look more deeply in this issue and to address these differences found in the spatial distribution of Z_{eu} and PP, a more representative data set of simultaneous bio-optical and PP data is necessary. The results presented here can support future campaigns by prioritizing areas of disagreement between approaches and poorly sampled regions to reduce uncertainty of PP in regional and global scales. In addition, special designed satellite missions using at least two quasi-polar orbits and same optical sensor could be considered. In this case, earlier (later) equator crossing time in descending (ascending) mode would increase signal to noise for the SO, thus reducing uncertainties of PP estimates.

Acknowledgements

We thank the Ocean Biology Processing Group of NASA for the distribution of the SeaWiFS and MODIS data. Thanks are also due to the Australian Antarctic Data Centre, LEFE-CYBER and PROOF program, SeaWiFS Bio-optical Archive and Storage System, United States JGOFS Data Server and Palmer Long-Term Ecological Research (LTER) for the public access to the *in situ* data. Data from the Palmer LTER data archive were supported by Office of Polar Programs, NSF

Grants OPP-9011927, OPP-9632763 and OPP-0217282. We are grateful to the many providers of the *in situ* data and Brenner Silva and Marc Taylor for discussions. We thank Christian Wolf and Wee Cheah for the sampling of absorption data during ANT-XXVI/3 and ANT-XXVIII/3, respectively, Sonja Wiegmann and Marta Kaspar for the analysis of these data and the principal scientists, crew and other scientists and students for the support during these two RV

Polarstern cruises. We also thank the two anonymous reviewers whose comments helped to improve the manuscript. The present work was conducted within the framework of the Helmholtz-University Young Investigators Group PHYTOOPTICS in cooperation with the Institute of Environmental Physics (University of Bremen) and Alfred Wegener Institute. The first author is supported by CAPES, Brazil, by the research grant BEX 3483/09-6.

Appendix A

Table A1
List of cruises.

Database	Cruise	Variables	Year
AADC ^a	Broke-West	Chla, Z _{eu}	2006
AADC	SAZ-Sense Voyage	Chla, Z _{eu}	2007
JGFOS ^b	Nbp97_8	Z _{eu}	1997
LEFE-CYBER ^c	Biosope	Chla, Z _{eu}	2004
PAL Ter ^d	PAL9798, PAL9899, LMG98-01, PAL9900, LMG99-01, LMG03-01, LMG05-01, PAL0607, LMG08-01	Chla, Z _{eu}	1998, 1999, 2003, 2003, 2006, 2008
SeaBASS ^e	nbp97_1 ^f , rev98_1 ^f , rev98_2 ^f	Z _{eu}	1997, 1998
SeaBASS	AMT 5, AMT6, AMT 6B, AMT 7, AMT 8	Chla, Z _{eu}	1997, 1998, 1999
SeaBASS	ROAVERRS ^f	Z _{eu}	1997, 1998
SeaBASS	Indoex ^f	Z _{eu}	1999
SeaBASS	AMLR ^f	Z _{eu}	2001, 2002, 2004, 2006, 2007, 2008
SeaBASS	LMG0402 ^f	Chla, Z _{eu}	2004
SeaBASS	Bencal02	Chla, Z _{eu}	2002
SeaBASS	NBP0606 ^f	Chla, Z _{eu}	2006
SeaBASS	i06s	Chla, Z _{eu}	2008
SeaBASS	SO_GASEX	a _{ph}	2008
SeaBASS	CLIVAR_p18	a _{ph}	2008
SeaBASS	CLIVAR_i8si9n	a _{ph}	2007
Own data set	ANT-XXVI/3	a _{ph}	2010
Own data set	ANT-XXVIII/3	a _{ph}	2012

^a Australian Antarctic Data Centre.
^b United States JGOFS Data Server.
^c http://www.obs-vlfr.fr/proof/index_vt.htm, French PROOF program.
^d Palmer Long-Term Ecological Research (LTER).
^e SeaWiFS Bio-optical Archive and Storage System (SeaBASS), Werdell et al. (2003).
^f Z_{eu} calculated by the authors from vertical profiles of PAR.

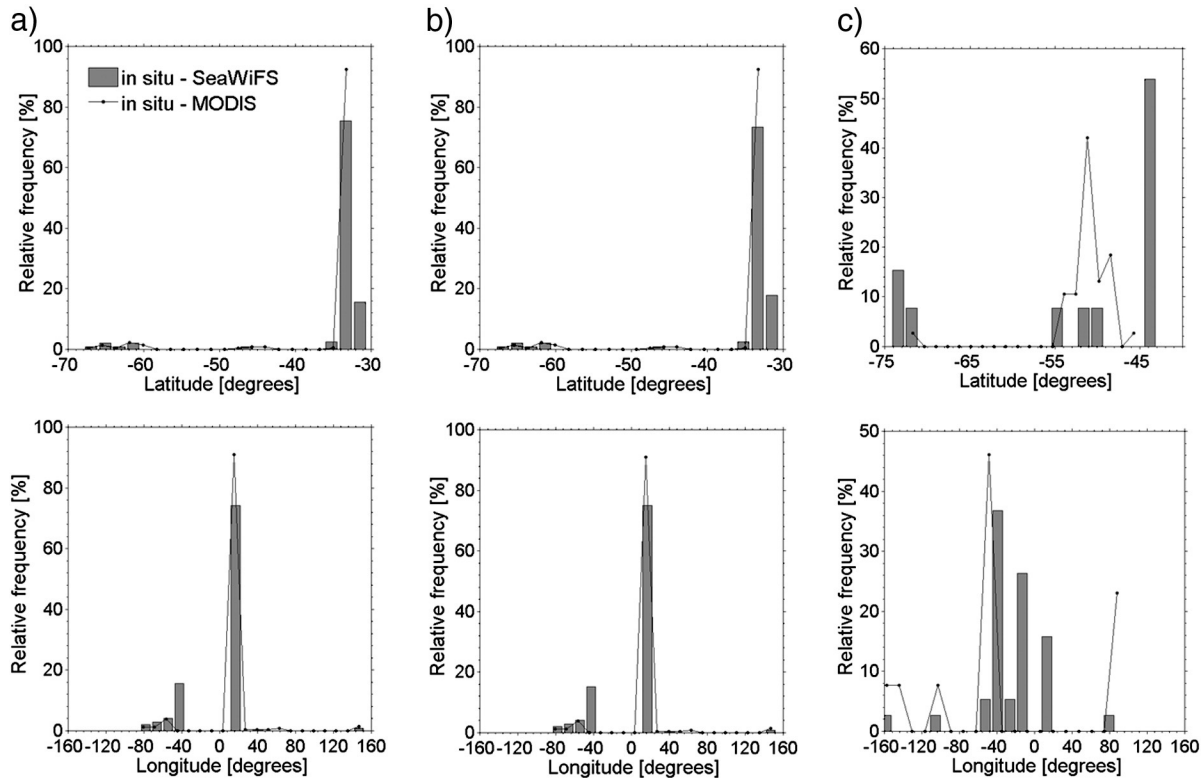


Fig. A1. Relative frequency distribution for *in situ*: (a) Z_{eu}, (b) Chla and (c) a_{ph} by latitude and longitude.

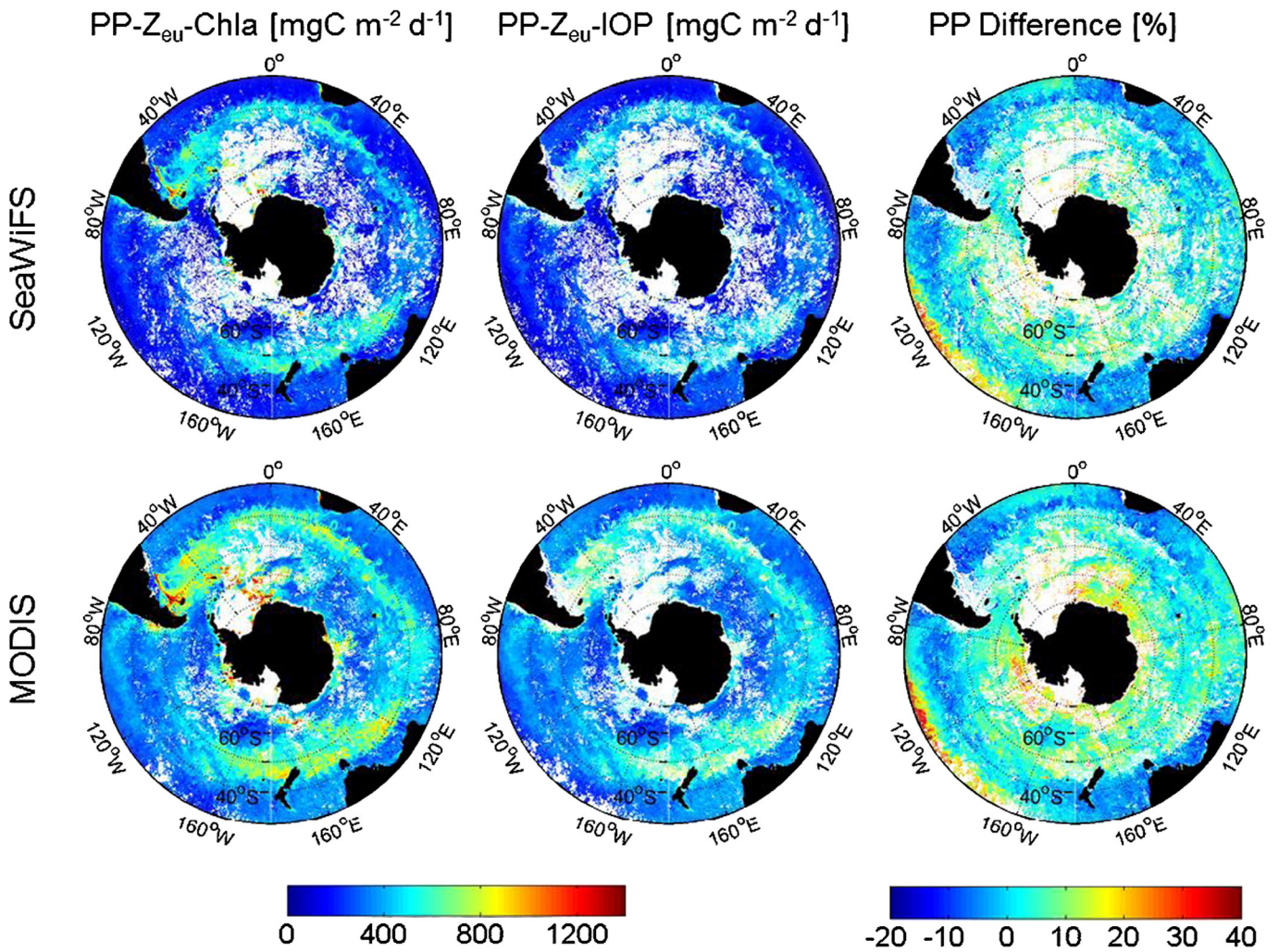


Fig. A4. Spatial distribution of PP in the Southern Ocean in February, 2003. PP-Z_{eu}-Chla (left), PP-Z_{eu}-IOP (right) and relative percentage of difference between PP-Z_{eu}-Chla and PP-Z_{eu}-IOP (center). The white pixels correspond to areas with no data.

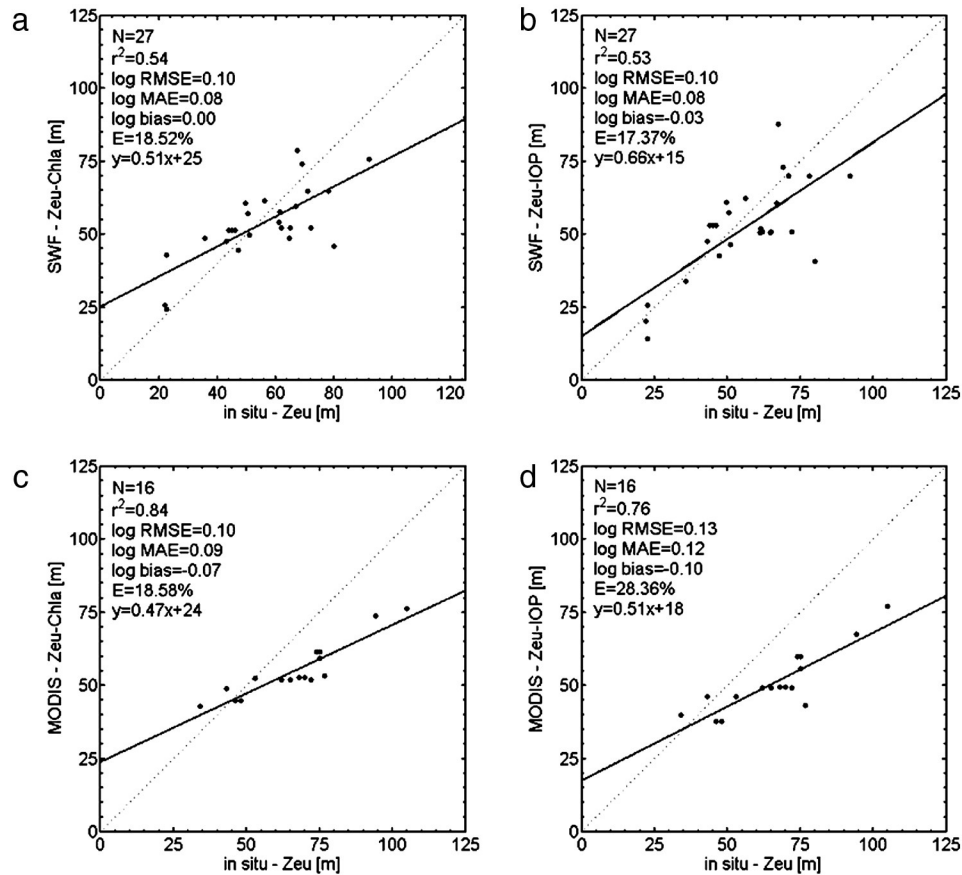


Fig. A5. Scatterplots of satellite Z_{eu} -Chla and Z_{eu} -IOP against *in situ* Z_{eu} south of 60°S. The solid line represents the regression and the dotted line represents the 1:1 line as reference.

References

- Arrigo, K. R., van Dijken, G., & Long, M. (2008). Coastal Southern Ocean: a strong anthropogenic CO_2 sink. *Geophysical Research Letters*, 35, L21602.
- Behrenfeld, M. J., & Falkowski, P. G. (1997). Photosynthetic rates derived from satellite-based chlorophyll concentration. *Limnology and Oceanography*, 42, 1–20.
- Belanger, S., Ehn, J. K., & Babin, M. (2007). Impact of sea ice on the retrieval of water-leaving reflectance, chlorophyll a concentration and inherent optical properties from satellite ocean color data. *Remote Sensing of Environment*, 111, 51–68.
- Campbell, J., Antoine, D., Armstrong, R., Arrigo, K., Balch, W., Barber, R., et al. (2002). Comparison of algorithms for estimating ocean primary production from surface chlorophyll, temperature, and irradiance. *Global Biogeochemical Cycles*, 16, 1035.
- Carr, M. -E., Friedrichs, M. A. M., Schmeltz, M., Noguchi Aita, M., Antoine, D., Arrigo, K. R., et al. (2006). A comparison of global estimates of marine primary production from ocean color. *Deep Sea Research Part II: Topical Studies in Oceanography*, 53, 741–770.
- Diessen, H., & Smith, R. (2000). Bio-optical properties and remote sensing ocean color algorithms for Antarctic Peninsula waters. *Journal of Geophysical Research*, 105, 26301–26312.
- Falkowski, P. G., & Raven, J. A. (2007). *Aquatic Photosynthesis* (2nd ed.) Princeton: Princeton University Press.
- Feldman, G. C., & McClain, C. R. (October 27). Ocean Color Chlorophyll (OC) v6, Ocean Color Web/Ocean Color Chlorophyll (OC) v6, Ocean Color Web. In N. Kuring, S. W. Bailey, B. F. Franz, G. Meister, P. J. Werdell, & R. E. Eplee (Eds.), : NASA Goddard Space Flight Center (12 December 2012). <http://oceancolor.gsfc.nasa.gov/REPROCESSING/R2009/ocv6/>.
- García, C. A. E., García, V. M. T., & McClain, C. R. (2005). Evaluation of SeaWiFS chlorophyll algorithms in the Southwestern Atlantic and Southern Oceans. *Remote Sensing of Environment*, 95, 125–137.
- Hirawake, T., Shinmyo, K., Fujiwara, A., & Saitoh, S. I. (2012). Satellite remote sensing of primary productivity in the Bering and Chukchi Seas using an absorption-based approach. *ICES Journal of Marine Science*, 69, 1194–1204.
- Hirawake, T., Takao, S., Horimoto, N., Ishimaru, T., Yamaguchi, Y., & Fukuchi, M. (2011). A phytoplankton absorption-based primary productivity model for remote sensing in the Southern Ocean. *Polar Biology*, 34, 291–302.
- Kahru, M., & Mitchell, B. G. (2010). Blending of ocean colour algorithms applied to the Southern Ocean. *Remote Sensing Letters*, 1, 119–124.
- Kirk, J. T. O. (2011). *Light and photosynthesis in aquatic ecosystems* (3rd ed.) Cambridge: Cambridge University Press.
- Lee, Z., Arnone, R., Hu, C., Werdell, P. J., & Lubac, B. (2010). Uncertainties of optical parameters and their propagations in an analytical ocean color inversion algorithm. *Applied Optics*, 49, 369–381.
- Lee, Z., Carder, K., & Arnone, R. (2006). The quasi-analytical algorithm. In Z. Lee (Ed.), *Remote Sensing of Inherent Optical Properties: Fundamentals, Tests of Algorithms, and Applications* (pp. 73–79). Dartmouth: International Ocean-Colour Coordinating Group.
- Lee, Z., Du, K., Arnone, R., Liew, A., & Penta, B. (2005). Penetration of solar radiation in the upper ocean: a numerical model for oceanic and coastal waters. *Journal of Geophysical Research*, 110, C09019.
- Lee, Z., Lance, V. P., Shang, S., Vaillancourt, R., Freeman, S., Lubac, B., et al. (2011). An assessment of optical properties and primary production derived from remote sensing in the Southern Ocean (SO GasEx). *Journal of Geophysical Research*, 116, C00F03.
- Lee, Z., Lubac, B., Werdell, J., & Arnone, R. (2009). An update of the quasi-analytical algorithm (QAA-v5), open file rep. available at: http://www.ioccg.org/groups/Software_OCA/QAA_v5.pdf (9 pp., (last access: 5 November 2012)).
- Lee, Z., Weidemann, A., Kindle, J., Arnone, R., Carder, K. L., & Davis, C. (2007). Euphotic zone depth: Its derivation and implication to ocean-color remote sensing. *Journal of Geophysical Research*, 112, C03009.
- Marrari, M., Hu, C., & Daly, K. (2006). Validation of SeaWiFS chlorophyll a concentrations in the Southern Ocean: A revisit. *Remote Sensing of Environment*, 105, 367–375.
- Mélin, F. (2011). Comparison of SeaWiFS and MODIS time series of inherent optical properties for the Adriatic Sea. *Ocean Science*, 7, 351–361.
- Morel, A., & Berthon, J. F. (1989). Surface pigments, algal biomass profiles, and potential production of the euphotic layer: relationships reinvestigated in view of remote-sensing applications. *Limnology and Oceanography*, 34, 1545–1562.
- Morel, A., Claustre, H., Antoine, D., & Gentili, B. (2007). Natural variability of bio-optical properties in Case 1 waters: attenuation and reflectance within the visible and near-UV spectral domains, as observed in South Pacific and Mediterranean waters. *Biogeosciences*, 4, 913–925.
- Morel, A., & Gentilini, B. (2004). Radiation transport within oceanic (case 1) water. *Journal of Geophysical Research: Oceans*, 109, C06008.
- O'Reilly, J. E., Maritorena, S., Siegel, D. A., O'Brien, M. C., Toole, D., Mitchell, B. G., et al. (2000). Ocean color chlorophyll algorithms for SeaWiFS, OC2, and OC4: Version 4. In S. B. Hooker, & E. R. Firestone (Eds.), *SeaWiFS Postlaunch Calibration and Validation Analyses, Part 3* (pp. 9–23). Maryland: NASA Goddard Space Flight Center.
- Saba, V. S., Friedrichs, M. A. M., Antoine, D., Armstrong, R. A., Asanuma, I., Behrenfeld, M. J., et al. (2011). An evaluation of ocean color model estimates of marine primary productivity in coastal and pelagic regions across the globe. *Biogeosciences*, 8, 489–503.

- Shang, S., Dong, Q., Lee, Z., Li, Y., & Behrenfeld, M. (2011). MODIS observed phytoplankton dynamics in the Taiwan Strait. *Biogeosciences*, 8, 841–850.
- Shang, S., Lee, Z., & Wei, G. (2011). Characterization of MODIS-derived euphotic zone depth: results for the China Sea. *Remote Sensing of Environment*, 115, 180–186.
- Szeto, M., Werdell, P. J., Moore, T. S., & Campbell, J. W. (2011). Are the world's oceans optically different? *Journal of Geophysical Research*, 116, C00H04.
- Takahashi, T., Sutherland, S. C., Wanninkhof, R., Sweeney, C., Feely, R. A., Chipman, D. W., et al. (2009). Climatological mean and decadal change in surface ocean pCO₂ and net sea–air CO₂ flux over the global oceans. *Deep Sea Research Part II: Topical Studies in Oceanography*, 56, 554–577.
- Taylor, B. B., Torrecilla, E., Bernhardt, A., Taylor, M. H., Peeken, I., Röttgers, R., et al. (2011). Bio-optical provinces in the eastern Atlantic Ocean and their biogeographical relevance. *Biogeosciences*, 8, 3609–3629.
- Thomalla, S. J., Fauchereau, N., Swart, S., & Monteiro, P. M. S. (2011). Regional scale characteristics of the seasonal cycle of chlorophyll in the Southern Ocean. *Biogeosciences*, 8, 2849–2866.
- Wang, M. H., & Shi, Wei (2009). Detection of ice and mixed ice–water pixels for MODIS ocean color data processing. *IEEE Transactions on Geoscience and Remote Sensing*, 47, 2510–2518.
- Werdell, P. J., Bailey, S. W., Fargion, G. S., Pietras, C., Knobelspiesse, K. D., Feldman, G. C., et al. (2003). Unique data repository facilitates ocean color satellite validation. *Eos, Transactions of the American Geophysical Union*, 84, 377.
- Willmott, C. J., & Matsuura, K. (2005). Advantages of the mean absolute error (MAE) over the root mean square error (RMSE) in assessing average model performance. *Climate Research*, 30, 79–82.
- Zibordi, G., Melin, F., & Berthon, J.-F. (2006). Comparison of SeaWiFS, MODIS and MERIS radiometric products at a coastal site. *Geophysical Research Letters*, 33, L06617.